



Electrochemiluminescence ultrasensitive immunoassay for carbohydrate antigen 125 based on AgInS₂/ZnS nanocrystals

Min Yin¹ · Yan Wang¹ · Xuwen Gao² · Shichao Du¹ · Yan Cheng¹ · Shuai Yu¹ · Guizheng Zou² · Fumin Xue¹

Received: 7 December 2020 / Revised: 14 January 2021 / Accepted: 20 January 2021 / Published online: 29 January 2021
© Springer-Verlag GmbH Germany, part of Springer Nature 2021

Abstract

We developed a near-infrared (NIR) electrochemiluminescence (ECL) immunosensor for sensitively and selectively determining carbohydrate antigen 125 (CA125) with toxic-element-free and environmental-friendly AgInS₂/ZnS nanocrystals (NCs) as tags. The core/shell-structured AgInS₂/ZnS NCs not only can be conveniently prepared via an aqueous synthetic procedure, but also has high photoluminescence quantum yield (PLQY) of up to 61.7%, highly monodispersed, water-soluble, and desired biological compatibility. As AgInS₂/ZnS NCs can be oxidized via electrochemically injecting holes into their valence band at + 0.84 V, both the monodispersed AgInS₂/ZnS NCs in solution and the surface-confined AgInS₂/ZnS NCs immobilized in sandwich-typed immuno-complexes with CA125 as analyte can exhibit efficient oxidative-reduction ECL around 695 nm under physiological conditions with the presence of tri-n-propylamine (TPrA). The ECL intensity from the AgInS₂/ZnS NCs immobilized in sandwich-typed immuno-complexes increases linearly and selectively with an increased concentration of CA125 from 5×10^{-6} to 5×10^{-3} U/mL, and limit of detection (LOD) was 1×10^{-6} U/mL (S/N = 3). This reliable platform can provide an effective detection method in the early diagnosis and treatment of ovarian cancer.

Keywords Electrochemiluminescence (ECL) · Immunosensor · AgInS₂/ZnS NCs · Carbohydrate antigen 125 (CA125)

Introduction

Electrochemiluminescence (ECL) is an emit light process in which an excited state-forming substance generated on the surface of an electrode undergoes an electron transfer reaction [1, 2]. ECL has attracted wide attention due to its low background, high sensitivity, electrochemical controllability, large sensing dynamic range, and superiority in fluorescence and sensitivity (S/N) [3]. The design and screening of ECL has played a vital role in the development after the preliminary study of ECL in 1964 [2]. The ECL phenomenon of

Ru(bpy)₃²⁺ and the anode co-reactant, tri-n-propylamine (TPrA) were discovered in 1972 and in 1987, respectively [4]. Then, the Ru(bpy)₃²⁺/TPrA system had been used as a commercial ECL detection system for the test of various life and medical diagnostic analytical field. Since Zou and Zhu reported in 2004 that CdSe NCs had made breakthroughs in ECL biosensors as ECL illuminants, a large number of binary NCs have been studied such as PbS [5], CdSe [6], and CdTe NCs [7]. Actually, the development of the lower toxic NCs was necessary to overcome the toxicity shortcoming of traditional II–IV NCs mentioned above [8].

In recent years, ternary metal chalcogenides (such as CuInS₂ and AgInS₂) have been recognized as promising light emitters with low biological toxicity [9], and have received a lot of research attention [10]. Studies showed that ternary metal chalcogenide nanocrystals had an adjustable band gap leading to adjustable optical properties [11]. It was reported that the core-shell-structured nanocrystals (such as CuInS₂/ZnS and AgInS₂/ZnS) showed a higher quantum yield than core CuInS₂ [12] or AgInS₂ [13]. This was related to the radiation recombination of ZnS with wide band gap after passivation of the core AgInS₂ surface [14, 15]. Due to the high carrier migration rate [16], ternary metal chalcogenide compounds were

Min Yin and Yan Wang contributed equally to this work.

✉ Fumin Xue
xuefumin@qlu.edu.cn

¹ School of Pharmaceutical Sciences, Shandong Analysis and Testing Center, Key Laboratory for Applied Technology of Sophisticated Analytical Instrument of Shandong Province, Qilu University of Technology (Shandong Academy of Sciences), Jinan 250014, Shandong, China

² School of Chemistry and Chemical Engineering, Shandong University, Jinan 250100, Shandong, China

widely used in photoelectric fields including solar cells [17] and light-emitting diodes [18]. More importantly, the surface of these nanocrystals can be easily modified with multifunctional ligands in preparation for binding to various target biomolecules [19], leading to the application in biological fields [20], such as bioimaging [21] and biosensors [22].

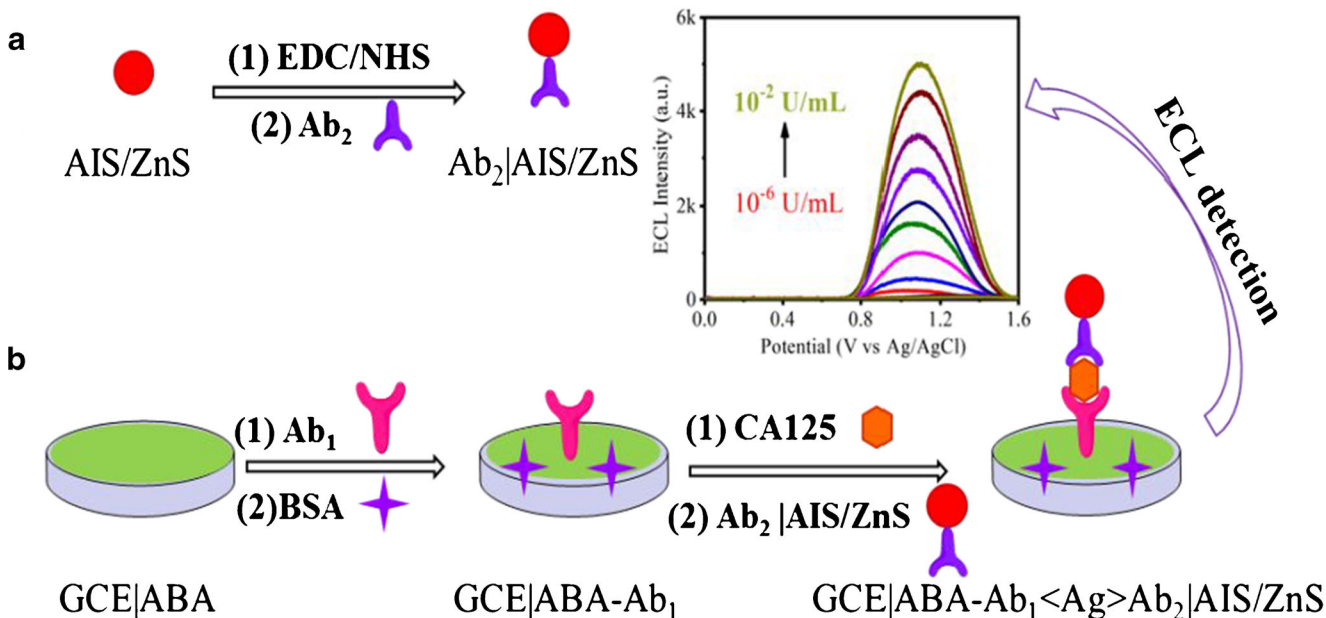
However, the researches about ECL immunoassay sensors fabricated by these ternary metal chalcogenide NCs to detect tumor markers are still limited. Herein, reduced glutathione and citric acid were used as stabilizers to prepare AgInS₂/ZnS NCs in the aqueous phase, whose ECL properties were studied with TPrA as the anode co-reactant [23]. Its ECL intensity is not only much greater than previously reported ternary NCs [24], but also produces a lower ECL potential, which can prohibit the electrochemical interference from high potential oxidation [25]. The water-phase AgInS₂/ZnS NCs exhibit excellent ECL performance, and the ECL immunodetection methods prepared with AgInS₂/ZnS NCs as markers can target CA125 at lower trigger potentials (Scheme 1). It would provide more effective detection methods in the early diagnosis and treatment of ovarian cancer. This work proposes an efficient nontoxic ECL immunosensing strategy with low trigger potential and less electrochemical interference, which was expected to be used for highly sensitive and selective bioassays.

Experimental

Chemicals and materials

All chemicals and materials were of analytical grade or better, and all aqueous solutions were prepared with double-distilled

water. Silver nitrate (AgNO₃, 99.8%) was purchased from Sinopharm Chemical Reagent Co., Ltd. (Shanghai, China). Potassium phosphate monobasic (KH₂PO₄) and isopropanol were purchased from Guangcheng Chemical Reagent Co., Ltd. (Tianjin, China). Sodium sulfide nonahydrate (Na₂S·9H₂O, 99.9%), ammonium hydroxide (NH₄OH), reduced glutathione (GSH) (98%), citric acid (99.5%), zinc acetate (Zn(CH₃COO)₂·2H₂O, 98%), indium trichloride tetrahydrate (InCl₃·4H₂O, 99.99%), p-aminobenzene formic acid (ABA), and TPrA were obtained from Aladdin (Shanghai, China). Potassium chloride (KCl), potassium ferricyanide (K₃[Fe(CN)₆]), potassium hexacyanoferrate (K₄[Fe(CN)₆]), and dipotassium hydrogen phosphate trihydrate (K₂HPO₄·3H₂O) were purchased from Xilong Chemical Co., Ltd. (Shantou, China). 1-Ethyl-3-(3-dimethylaminopropyl) carbodiimide hydrochloride (EDC, 98%) and bovine serum albumin (BSA) were purchased from Sigma-Aldrich Chemicals Co. LLC. (St. Louis, MO, USA). N-Hydroxysuccinimide (NHS) was obtained from Sinopharm Chemical Reagent Co., Ltd. (Shanghai, China). EDC and NHS were dissolved in a 100 mM pH 7.4 phosphate buffer (PB) containing 0.50 M KCl before use. Carbohydrate antigen 125 (CA125, Ag, 50KU/ml, Lot: 181120), capture CA125 antibody (2.7 mg/mL, Ab₁, Lot: Z811N206), probe CA125 antibody (2.8 mg/mL, Ab₂, Lot: Z811N204), alpha-fetoprotein (AFP, 105 μg/mL, Ag, Lot: 120715), carcinoembryonic antigen (CEA 100 μg/mL, Ag, Lot: 170210), and prostate-specific (PSA) (PSA, 0.1 mg/mL, Ag, Lot: 191130), antigen and antibody were purchased from Beijing Keyue Zhongkai Biotechnology Co., Ltd., (Beijing, China), which were diluted with 10 mM pH 7.4 PB before use. The human serum samples in this study were bought from Beijing Century Aoke Biotechnology Co., Ltd. (Beijing, China).



Scheme 1 Schematic illustration of the fabricating procedures of ECL sensor with AgInS₂/ZnS NCs as tag

Apparatus

Ultraviolet-visible (UV-vis) absorption and photoluminescence (PL) spectra were recorded on ultraviolet-visible Lambda365 spectrophotometer (PerkinElmer, South Korea) and F-4600 fluorescence spectrophotometer (Hitachi, Japan), respectively. PL lifetime and PL quantum yield (PLQY) of colloidal AgInS₂/ZnS NCs were carried on an FLS920 fluorescence spectrometer (Edinburgh Instruments, UK). High-resolution transmission electron microscope (HRTEM) image was taken on the Titan G2 60-300 transmission electron microscope (FEI, USA). X-ray diffraction (XRD) pattern was recorded on ultima IV X-ray diffractometer within an angle 2θ range from 20° to 70° (Rigaku Beijing Corp, China). X-ray photoelectron spectroscopy (XPS) was collected on Thermo ESCALAB 250Xi X-ray photoelectron spectroscopy (Thermo Fisher Scientific, USA). Differential pulse voltammetry (DPV) curves were recorded with a CHI 760E electrochemical analyzer (Shanghai, China). Cyclic voltammograms (CV) and ECL measurements were carried out on an MPI-EII ECL analyzer (Xi'an Remex Analytical Instrument Co., Ltd., China). ECL spectra were accomplished with a homemade ECL spectrometer consisting of an Acton SP2300i monochromator equipped with a VersaSTAT 3 electrochemical analyzer (Princeton Applied Research, USA) and a liquid N₂ cooled PyLoN 400BR-eXcelon digital CCD detector (Princeton Instruments, USA) by using a three-electrode system, including a Pt coil counter electrode, an Ag/AgCl containing saturated KCl reference electrode, and a 5 mm diameter glassy carbon electrode (GCE).

Preparation of AgInS₂/ZnS NCs

Colloidal AgInS₂/ZnS NCs were synthesized in the aqueous phase by using GSH and citric acid as stabilizers [23] [21]. Typically, a 2.5 mL double-distilled water combining an aliquot of GSH (0.5 M, 2.4 mL) and InCl₃·4H₂O (1.0 M, 0.8 mL) containing 0.25 M HNO₃ were vigorously stirred in a three-necked flask to be dissolved completely. After ~3 min, NH₄OH (5.0 M, 1.0 mL) was added and stirred until the white precipitate was dissolved. Subsequently, AgNO₃ (0.1 M, 2 mL), Na₂S·9H₂O (1.0 M, 1.0 mL), and citric acid (2.0 M, 0.25 mL) were rapidly injected into the mixture to react for 60 min at 98 °C and form AgInS₂ NCs. Meanwhile, GSH (0.5 M, 3.0 mL) was stirred with NH₄OH (5.0 M, 0.4 mL) and Zn(CH₃COO)₂·2H₂O (1.0 mM, 1.6 mL) containing 0.01 M HNO₃ to form a clear solution, and the solution was stirred with the above-prepared AgInS₂ colloid, and reacted for 10 min at 98 °C to obtain AgInS₂/ZnS NCs. Finally, the AgInS₂/ZnS NCs was centrifuged and washed with isopropanol at 10000 rcf for three times, and then dispersed

in double-distilled water at 4 °C to obtained monodispersed AgInS₂/ZnS NCs.

Preparation of AgInS₂/ZnS NC-labeled CA125 antibody (i.e., CA125 Ab₂|AgInS₂/ZnS)

As demonstrated in Scheme 1a, the carboxylic groups of AgInS₂/ZnS NCs was activated by mixing 50 μL purified AgInS₂/ZnS NCs with an aliquot of 20 μL pH 6.0 PB containing 100 mg/mL EDC and 100 mg/mL NHS for 30 min at room temperature, and then centrifuged at 12000 rcf for 6 min. The precipitate was re-dispersed in 1.0 mL 10 mM pH 7.4 PB containing 10 μg/mL CA125 Ab₂ to form CA125 Ab₂|AgInS₂/ZnS conjugates. Then, 10 μL 1% (v/v) BSA was added to block the nonspecific binding sites for 30 min after shaking for 3 h at room temperature. Finally, the CA125 Ab₂|AgInS₂/ZnS conjugates was centrifuged and re-dispersed in 1.0 mL 10 mM pH 7.4 PB, and stored at 4 °C for further use.

Preparation of AgInS₂/ZnS NC-based ECL biosensor

According to Scheme 1b, the ECL immunosensor was fabricated with AgInS₂/ZnS NCs initialed by immobilizing antibody (Ab₁) onto the GCE with ABA as adapter [26]. The GCE was polished to a mirror with alumina slurry, washed cleanly with a lot of double-distilled water, and dried by nitrogen (N₂). Subsequently, the cleaned GCE was electrodeposited with 1.0 mM ABA by scanning potential from 0.4 to 1.2 V in 0.1 M pH 7.4 PB containing 1.0 mM ABA at 10 mV/s for three cycles to form carboxyl group-modified GCE|ABA [25]. The carboxyl groups of GCE surface were activated with 100 mg/mL EDC and 100 mg/mL NHS at room temperature after the GCE|ABA was washed with ethanol and double-distilled water. The GCE|ABA was placed into 10 mM pH 7.4 PB containing 10 μg/mL CA125 Ab₁ for 2 h to form GCE|ABA-CA125 Ab₁. The electrode was washed with 10 mM pH 7.4 PB, and then 1% (v/v) BSA solution was added dropwise for 30 min to block any remaining activated carboxyl groups. The GCE|ABA-CA125 Ab₁ was then incubated with an aliquot of 20 μL CA125 antigen with different concentrations for 90 min at 37 °C to obtain GCE|ABA-CA125 Ab₁<CA125 antigen>. The GCE|ABA-CA125 Ab₁<CA125 antigen> was further incubated with CA125 Ab₂|AgInS₂/ZnS for 1 h to form a sandwich-type immunosensor, i.e., GCE|ABA-CA125 Ab₁<CA125 antigen>CA125 Ab₂|AgInS₂/ZnS.

ECL detection of CA125

The ECL immunosensor measurements were detected in 0.1 M pH 7.4 PB containing 10 mM TPra by scanning

potential from 0 to 1.6 V for one cycle at 50 mV/s. Serum samples were diluted with 10 mM pH 7.4 PB to determine CA125. The voltage of photomultiplier tube was set to 800 V during ECL detection.

Results and discussion

Characterization of AgInS₂/ZnS NCs

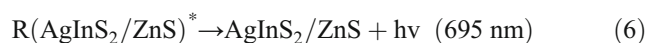
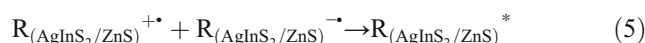
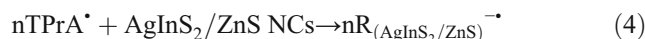
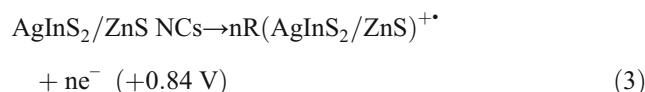
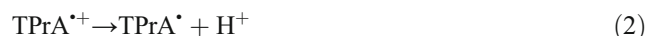
The PL spectrum of as-prepared dual-stabilizer-capped AgInS₂/ZnS NCs with GSH and citric acid was characterized by a broad and symmetric PL band in the visible and near-infrared (NIR) region with maximum emission around 635 nm and full-width at half-maximum (FWHM) of 100 nm (Fig. 1A). It was similar to that of previously reported results, and this PL band originated to a large extent from inhomogeneous PL broadening [23]. The UV-vis absorption spectrum of AgInS₂/ZnS NCs was featureless. It was worth noting that PLQY of AgInS₂/ZnS NCs we prepared is as high as 61.7%. The PL decay curve of AgInS₂/ZnS NCs could be well-fitted by a tri-exponential function (Fig. 1B), and the lifetime was as high as 1.8 μs (see Supplementary Information (ESM) Table S1), which can be attributed to the intrinsic defects and surface defects [27]. The multiexponential decay kinetics were PL properties inherent for these types of NCs and originate from the complicated structure of the low-energy states of the AgInS₂/ZnS NCs [28].

The XRD pattern demonstrated three main diffraction peaks with their 2θ value of 27.09°, 45.57°, and 53.54° located between cubic AgInS₂ and ZnS respectively (Fig. 1C), which proved the successful preparation of the core-shell structure of AgInS₂/ZnS NCs [23]. The HRTEM pattern showed that the AgInS₂/ZnS NCs were spherical particles with an average size about 5 nm (Fig. 1D). They are uniformly monodispersed, which provided a basic condition for the subsequent biosensor application. The XPS patterns further confirm that AgInS₂/ZnS NCs were composed of Ag, In, S, and Zn (ESM Fig. S1), and the element ratio of Ag: In: S: Zn was 0.33: 0.745: 2.18: 1.34, indicating the synthesis of AgInS₂/ZnS NCs.

Co-reactant ECL of AgInS₂/ZnS NCs in aqueous medium

The anode co-reactant, TPrA, can bring out oxidative-reduction ECL of NCs via electrochemical oxidation to produce strongly reducing radical species TPrA[•], and can also avoid the possible interference of dissolved oxygen. As shown in Fig. 2B, no obvious ECL was observed from bare GCE in 0.1 M pH 7.4 PB containing 10 mM TPrA (curve a, Fig. 2B), while the monodispersed AgInS₂/ZnS NCs in aqueous

medium exhibited efficient ECL emission with peak at 0.84 V (curve b, Fig. 2B) [29]. DPV was used to verify the accurate hole injection process of the AgInS₂/ZnS NCs. The DPV curve of AgInS₂/ZnS NCs displayed a hole-injecting process around 0.84 V (inset A of Fig. 2A). Hence, AgInS₂/ZnS NCs can be electrochemically oxidized to one hole-charged state at 0.84 V. Forming a wide band gap ZnS shell around the AgInS₂ core would make the AgInS₂ core less sensitive to external environment and the hole injection process caused by electrochemical oxidation was critical for the formation of AgInS₂/ZnS NCs redox ECL. The ECL spectrum of AgInS₂/ZnS NCs containing TPrA showed obvious ECL signal with the maximum emission wavelength of 695 nm (inset B of Fig. 2B), and the ECL spectrum of AgInS₂/ZnS NCs exhibited a red shift compared with PL spectrum. It suggests that the surface defects were not fully passivated in the redox carrier migration of anode ECL and hinder the radiation charge transfer during hole injection (ESM Fig. S2A) [30].



The valence bands (VB) of AgInS₂/ZnS NCs can be injected with holes to produce NCs of hole-injected states (AgInS₂/ZnS^{•+}) via electrochemically oxidizing them respectively (Eq. 3), while the conduction band (CB) of AgInS₂/ZnS NCs can be injected with electrons to produce NCs of electron-injected states via reducing the NCs with strong reducing radical TPrA[•] (eq. 4). The TPrA[•] is generated via electrochemically oxidizing TPrA (Eqs. 1 and 2). The radiative charge transfer/recombination between NCs of hole-injected and electron-injected states eventually produce NCs of excited states for ECL (Eqs. 5 and 6).

Characterization of AgInS₂/ZnS NCs and the Ab₂-AgInS₂/ZnS conjugates

The ECL spectrum of AgInS₂/ZnS NCs/TPrA showed a broad peak with maximum wavelength at 695 nm (curve b, ESM Fig. S2A). The ECL of AgInS₂/ZnS NCs/TPrA was red shifted by ~60 nm with respect to AgInS₂/ZnS NCs PL spectrum (curve a, ESM Fig. S2A) and has a similar color to the ECL of Ru(bpy)₃²⁺/TPrA. These results indicated that surface

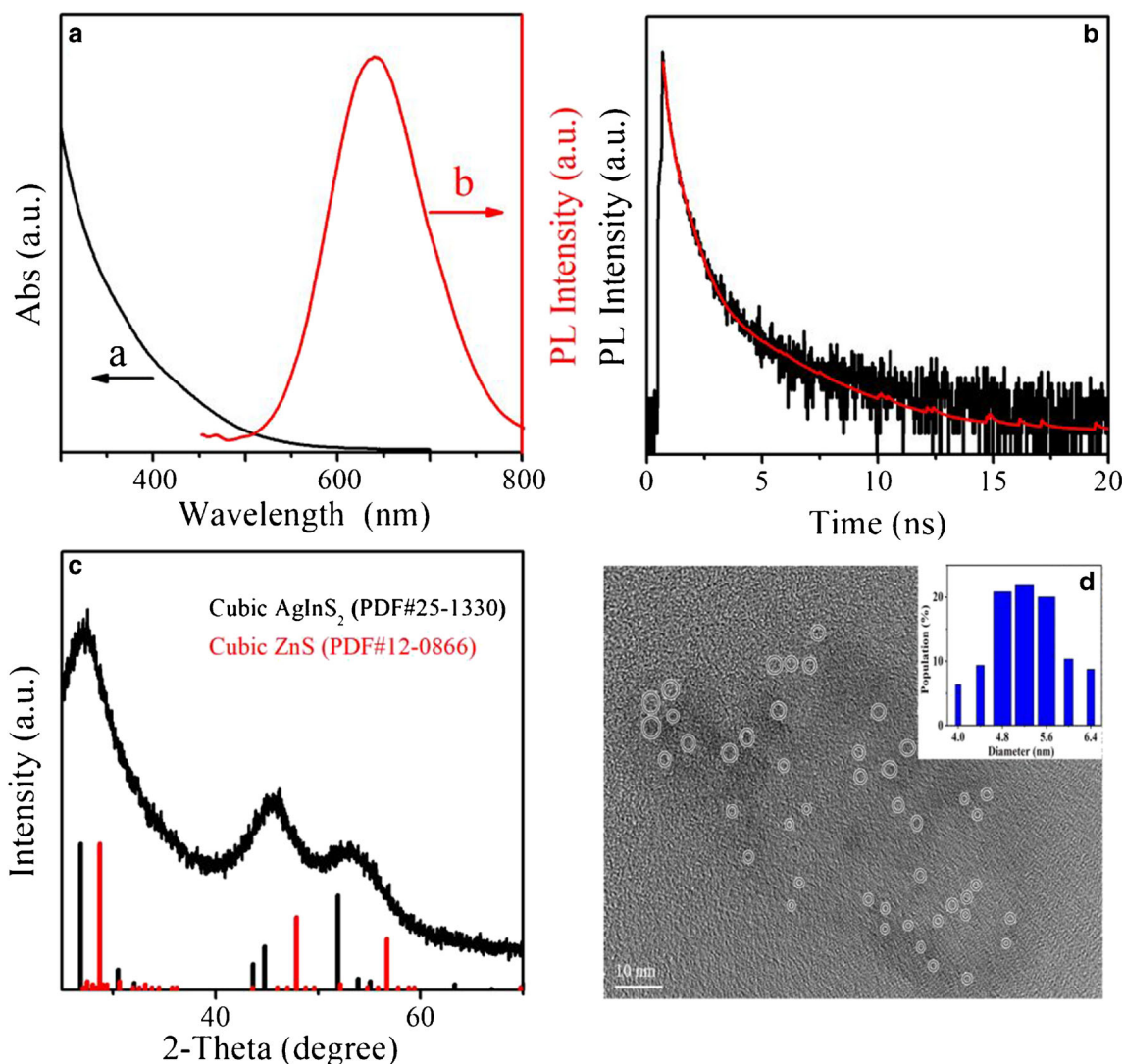


Fig. 1 (A) UV-vis absorption (a, black line) and PL (b, red line) spectra, (B) PL decay curve, (C) XRD pattern, and (D) HRTEM image and size distribution patterns (inset) of AgInS₂/ZnS NCs

defects still played an important role in the electrochemical redox-induced radiative charge transfer of AgInS₂/ZnS NCs. Importantly, the ECL spectrum of surface-confined AgInS₂/ZnS NCs on GCE|ABA-Ab₁<CA125>Ab₂-AgInS₂/ZnS was almost the same as that of monodispersed AgInS₂/ZnS NCs with maximum emission around 95 nm (curves b and c, ESM Fig. S2A). This indicates that the L-glutathione- and citrate-stabilized AgInS₂/ZnS NCs preserved their surface states very well via complicated labeling and bioreaction processes, and AgInS₂/ZnS NCs was expected to be used for ECL labeling in biological assay.

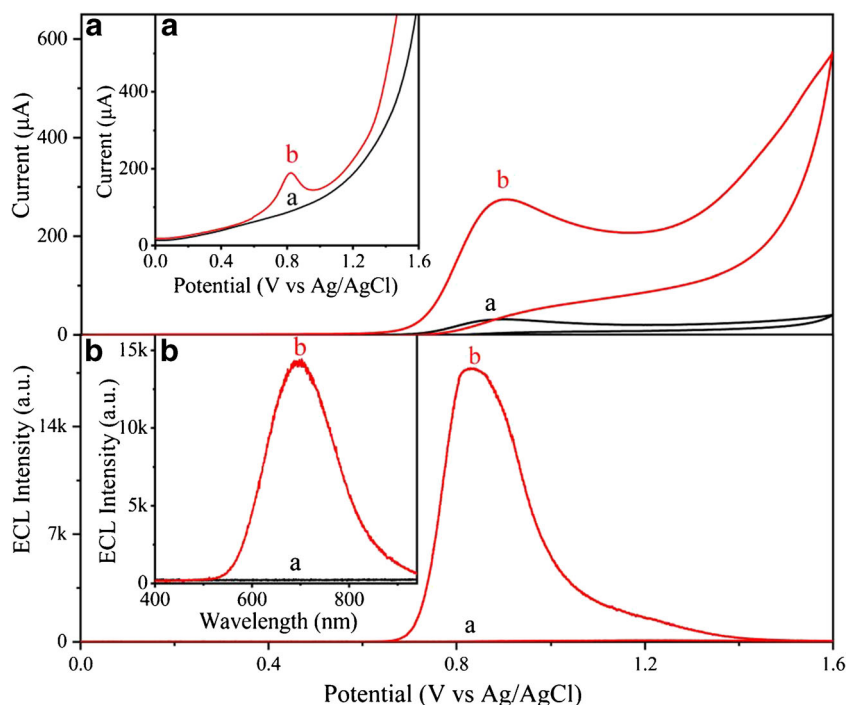
As shown in Fig. S2B, both AgInS₂/ZnS NCs and Ab₂-AgInS₂/ZnS conjugates revealed effective ECL in 0.10 M pH 7.4 PB containing 10 mM TPrA. This undoubtedly showed that the ECL of AgInS₂/ZnS NCs and Ab₂-AgInS₂/ZnS conjugates followed the typical ECL method of anode co-reactant. The Ab₂-AgInS₂/ZnS conjugate showed a good

ECL-potential distribution at 0.0 v-1.6 v, although Ab₂ might hinder the hole (or electron) injection process on the surface of AgInS₂/ZnS NCs, resulting in lower ECL strength and higher potential compared with AgInS₂/ZnS NCs.

Characterization of the ECL sensor with AgInS₂/ZnS as tags

The fabrication procedure of ECL immunosensor, GCE|ABA-CA125 Ab₁<CA125 antigen>CA125 Ab₂-AgInS₂/ZnS, was characterized with an equimolar mixture of 5.0 mM Fe(CN)₆³⁻/Fe(CN)₆⁴⁻ redox couple in 0.10 M pH 7.4 PB as previously reported (Fig. 3A). The bare GCE showed a pair of symmetrical reversible with redox peak potential separation (ΔE_p) of 70 mV (curve a). The ΔE_p was increased significantly and the peak currents are dropped sharply after ABA was deposited on the surface of the GCE, which can be

Fig. 2 (A) CV and (B) ECL profiles of (a) bare GCE and (b) 0.5 mg/mL AgInS₂/ZnS NCs in 0.1 M pH 7.4 PB containing 10 mM TPrA at 50 mV/s. Inset of A: DPV profiles of (a) bare GCE and (b) 0.5 mg/mL AgInS₂/ZnS NCs in 0.1 M pH 7.4 PB. Inset of B: Corresponding ECL spectra of Fig. 2B by collecting all the photons generated via scanning the potential from 0 to 1.6 V for one cycle at 50 mV/s



attributed to the electrostatic repulsion of $\text{Fe}(\text{CN})_6^{3-}/\text{Fe}(\text{CN})_6^{4-}$ and ABA with negative charge. A decrease of ΔE_p with increased current was observed after ABA|GCE was immobilized with Ab₁ and treated with BSA (curve c), because of the decrease in the effective surface area of ABA|GCE and partially restored redox of $\text{Fe}(\text{CN})_6^{3-}/\text{Fe}(\text{CN})_6^{4-}$ couple. The currents of redox peak decrease obviously with the increase of ΔE_p after further modification of antigen (curve d) and Ab₂|AgInS₂/ZnS (curve e). The redox electron transfer of the redox probes was blocked with the formation of larger molecular weight immune complexes with bigger steric hindrance, demonstrating the assembly of the sandwich-type ECL immunosensors as expected.

According to Fig. 3B, no ECL signal was observed with bare GCE (curve a), GCE|ABA (curve b), GCE|ABA-Ab₁ (curve c), and GCE|ABA-Ab₁<CA125 antigen> (curve d) in 0.1 M pH 7.4 PB containing 10 mM TPrA, but the GCE|ABA-Ab₁<CA125 antigen>Ab₂|AgInS₂/ZnS (curve e) exhibited efficient ECL in the same solution. It provides an unambiguous evidence that AgInS₂/ZnS NCs was immobilized onto GCE surface via the proposed sandwich-typed immunosensing strategy [31].

Bioassay performance of ECL of AgInS₂/ZnS NCs

According to Fig. 4, ECL-potential profiles of GCE|ABA-CA125 Ab₁<CA125 antigen>CA125 Ab₂|AgInS₂/ZnS

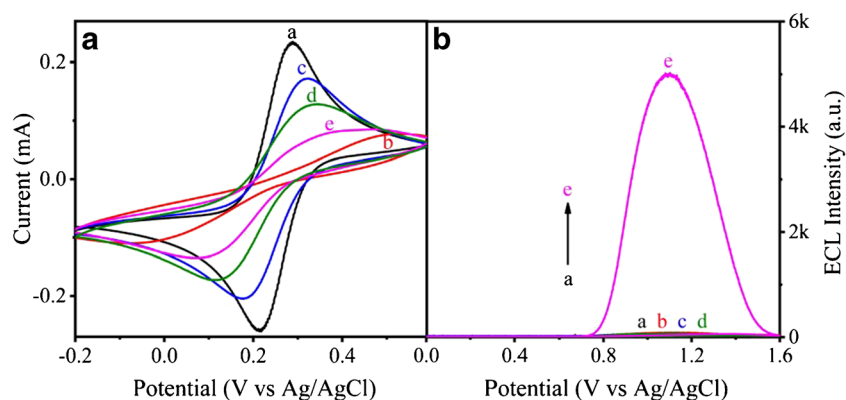


Fig. 3 (A) CV behaviors of (a) bare GCE, (b) GCE|ABA, (c) GCE|ABA-Ab₁, (d) GCE|ABA-Ab₁<CA125, and (e) GCE|ABA-Ab₁<CA125>Ab₂-AgInS₂/ZnS in 0.1 M pH 7.4 PB containing 5.0 mM K₃Fe(CN)₆/K₄Fe(CN)₆. (B) ECL profiles of (a) bare GCE, (b) GCE|ABA, (c)

GCE|ABA-Ab₁, (d) GCE|ABA-Ab₁<CA125, and (e) GCE|ABA-Ab₁<CA125>Ab₂-AgInS₂/ZnS in 0.1 M pH 7.4 PB containing 10 mM TPrA at 50 mV/s. The concentration of CA125 sample was 10⁻² U/mL

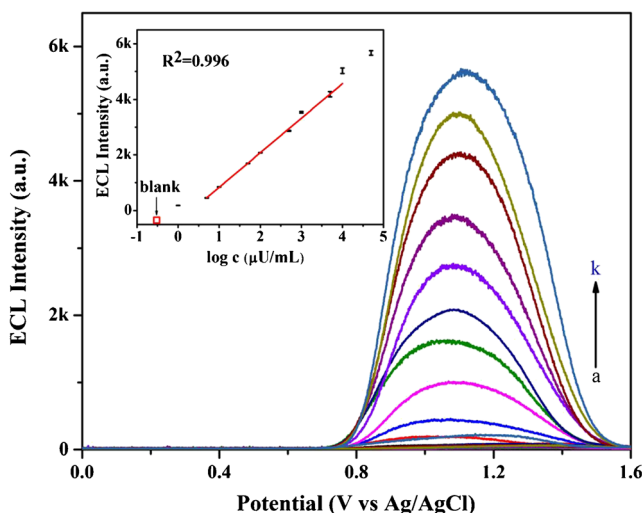


Fig. 4 ECL profiles of GCE|ABA-Ab₁<CA125>Ab₂-AgInS₂/ZnS formed with (a) 0.0, (b) 10⁻⁶, (c) 5 × 10⁻⁶, (d) 10⁻⁵, (e) 5 × 10⁻⁵, (f) 10⁻⁴, (g) 5 × 10⁻⁴, (h) 10⁻³, (i) 5 × 10⁻³, (j) 10⁻², (k) 5 × 10⁻² U/mL CA125 by collecting all the photons generated via scanning the sensor in 0.1 M pH 7.4 PB containing 10 mM TPrA from 0 to 1.6 V for one cycle at 50 mV/s. Inset: corresponding calibration curve for CA125 determination

formed with different concentrations of CA125 sample were similar to each other with peak potential around 1.08 V. The spectral ECL response of GCE|ABA-CA125 Ab₁<CA125 antigen>CA125 Ab₂|AgInS₂/ZnS increases gradually along with the incremental of CA125 concentration. The linear correlation between the peak potential of ECL-potential profiles and the logarithmic concentration of CA125 was obtained from 5 × 10⁻⁶ ~ 5 × 10⁻³ U/mL. Higher or lower concentration will deviate from the linear range. For example, in Fig. 4, when the concentration of the antigen to be detected was 5 × 10⁻² U/mL or 10⁻² U/mL, the linearity will deviate. Under the following conditions, the detection limit (LOD) was 10⁻⁶ U/mL, and the signal-to-noise ratio (S/N) was 3.

The performance of GCE|ABA-CA125 Ab₁<CA125 antigen>CA125 Ab₂|AgInS₂/ZnS for determining CA125 was comparable with even higher ECL response, lower potential, and more sensitive than some recently reported ECL, DPV, EIS, chronoamperometry (CAMP), fluorescence assays compared to other ternary I-III-IV NCs (ESM Table S1) [32–37]. It was certain that the biosensor we developed has a significant improvement over other methods in the ultrasensitive detection of CA125.

Characteristics of ECL biosensor based on AgInS₂/ZnS NCs

Reproducibility of the ECL-potential immunosensor was tested at a set of CA125 concentrations, and each of them was repeated for five times (Fig. 5A). The maximum relative standard deviation of the ECL intensity at peak potential of GCE|ABA-CA125 Ab₁<CA125 antigen>CA125 Ab₂|AgInS₂/ZnS of the same concentration was 5.7%. This clearly demonstrates that the preparation of ECL sensor has good reproducibility and feasibility of potential-based ECL analysis with AgInS₂/ZnS NCs as label. In addition, no obvious ECL was detected with GCE|ABA-CA125 Ab₁<CA125 antigen>CA125 Ab₂|AgInS₂/ZnS formed via the pure blank sample or the CA125 blank sample containing some other high concentration interfering proteins, such as PSA, CEA, and BSA (Fig. 5B). The efficient ECL response with the sample only containing with 10⁻⁴ U/mL CA125, which indicates that GCE|ABA-CA125 Ab₁<CA125 antigen>CA125 Ab₂|AgInS₂/ZnS, was highly specific to the target molecule CA125. In addition, compared with the sample containing only 1 × 10⁻⁴ U/mL CA125, it contained 1 × 10⁻⁴ U/mL CA125 and several other three interfering proteins (such as PSA, CEA, and BSA) at the same level. The mixture sample

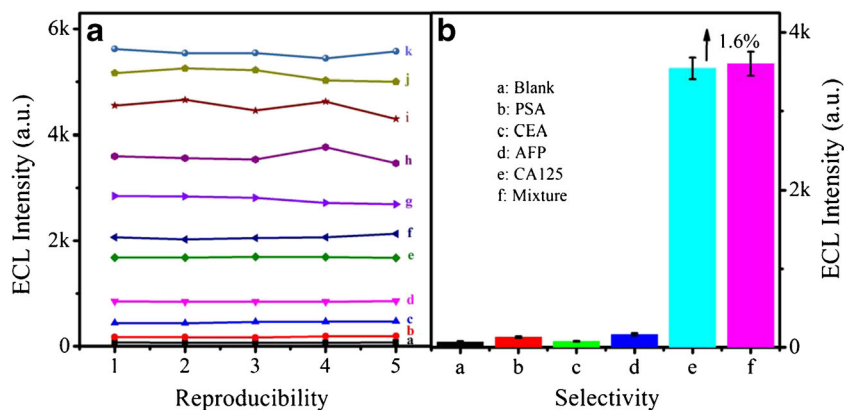


Fig. 5 (A) Parallel tests for CA125 determination by the maximum intensity on the ECL profiles of GCE|ABA-Ab₁<CA125>Ab₂-AgInS₂/ZnS formed with CA125 at (a) 0.0, (b) 10⁻⁶, (c) 5 × 10⁻⁶, (d) 10⁻⁵, (e) 5 × 10⁻⁵, (f) 10⁻⁴, (g) 5 × 10⁻⁴, (h) 10⁻³, (i) 5 × 10⁻³, (j) 10⁻², (k) 5 × 10⁻² U/mL levels, respectively. (B) The specificity of the ECL immunoassay.

The bars represent the maximum emission on ECL profiles of GCE|ABA-Ab₁<CA125>Ab₂-AgInS₂/ZnS formed with (a) blank, (b) 1 μg/mL PSA, (c) 1 μg/mL CEA, (d) 1 μg/mL AFP, (e) 10⁻⁴ U/mL CA125, respectively, and (f) the mixture of above

will only bring out slightly increased ECL response (~ 1.6%). It was clear that GCE|ABA-CA125 Ab₁<CA125 antigen>CA125 Ab₂|AgInS₂/ZnS also exhibited acceptable specificity.

Real sample analysis

The standard addition method was used to detect human serum samples to verify the accuracy and analytical reliability of the constructed ECL immunosensor. The concentration of CA125 in the actual sample was 20 U/mL, and we diluted the serum sample with 10 mM PBS to 0.20 mU/mL to make the concentration within the range of the standard curve. As shown in ESM Table S3, the relative standard deviation (RSD) of human serum samples were 6.22%, 6.52%, and 2.58%, respectively. The average recovery rates were 100.4%, 99.9%, and 101.2%, respectively. The results showed that the method has high accuracy, and the prepared ECL immunosensor can be better applied to detection in actual samples.

Conclusions

In summary, a convenient ECL biosensor for detecting tumor marker CA125 of ovarian cancer was developed, in which nontoxic AgInS₂/ZnS NCs in aqueous medium used as ECL illuminant exhibited excellent ECL performance with the existence of co-reactant TPrA. It should be noted that the AgInS₂/ZnS NCs could be electrochemically oxidized to hole-injected states at 0.84 V, and co-reactant-type ECL was generated with TPrA through carrier migration. The bio-label can determine CA125 from 5×10^{-6} to 5×10^{-3} U/mL with the limit of detection at 1×10^{-6} U/mL ($S/N=3$). The novel ECL immunosensing strategy based on ternary metal chalcogenides at low ECL triggering potential would provide an easy-to-use, sensitive, and reliable platform for detecting tumor markers in clinical samples as an ultrasensitive analytical technique.

Supplementary Information The online version contains supplementary material available at <https://doi.org/10.1007/s00216-021-03191-0>.

Funding The work in this paper received support from the Shandong Keypoint Research & Development Plan (grant references: 2018GSF117006, and 2019GSF109063), Shandong Province TaiShan Scholar Program (ts20190948), and the National Natural Science Foundation of China (NSFC) (grant references: 21703126).

Declarations The human serum samples in this study were bought from Beijing Century Aoke Biotechnology Co., Ltd. (Beijing, China). In addition, these studies were approved by the ethics committee of Qilu University of Technology, and in accordance with the ethical standards “Qilu University of Technology” and with the 1964 declaration of Helsinki and its later amendments or comparable ethical standards.

Conflict of interest The authors declare no conflict of interest.

References

- Richter MM. Electrochemiluminescence (ECL). *Chem Rev.* 2004;104(6):3003–36.
- Visco RE, Chandross EA. Electroluminescence in solutions of aromatic hydrocarbons. *J Am Chem Soc.* 1964;86(23):5350–1.
- Wu L, Sha Y, Li W, Wang S, Guo Z, Zhou J, et al. One-step preparation of disposable multi-functionalized g-C₃N₄ based electrochemiluminescence immunosensor for the detection of CA125. *Sensors Actuators B Chem.* 2016;226:62–8.
- Diez I, Pusa M, Kulmala S, Jiang H, Walther A, Goldmann AS, et al. Color tunability and electrochemiluminescence of silver nanoclusters. *Angew Chem Int Ed.* 2009;48(12):2122–5.
- Sha H, Wang Y, Zhang Y, Ke H, Xiong X, Jia N. Enzyme-free ECL immunosensor based on PbS nanocrystals for highly sensitive detection of alpha fetoprotein. *Sensors Actuators B Chem.* 2018;277:157–63.
- Zhang F, He Y, Fu K, Fu L, Zhang B, Wang H, et al. Dual-wavebands-resolved electrochemiluminescence multiplexing immunoassay with dichroic mirror assistant photomultiplier-tubes as detectors. *Biosens Bioelectron.* 2018;115:77–82.
- Gao X, Fu K, Fu L, Wang H, Zhang B, Zou G. Red-shifted electrochemiluminescence of CdTe nanocrystals via Co²⁺-doping and its spectral sensing application in near-infrared region. *Biosens Bioelectron.* 2020;150:111880.
- Nelson HD, Gamelin DR. Valence-band electronic structures of Cu⁺-doped ZnS, alloyed Cu–In–Zn–S, and ternary CuInS₂ nanocrystals: a unified description of photoluminescence across compositions. *J Phys Chem C.* 2018;122(31):18124–33.
- Pan ZX, Mora-Sero I, Shen Q, Zhang H, Li Y, Zhao K, et al. High-efficiency “green” quantum dot solar cell. *J Am Chem Soc.* 2014;136(25):9203–10.
- Allen PM, Bawendi MG. Ternary I-III-VI quantum dots luminescent in the red to near-infrared. *J Am Chem Soc.* 2008;130(29):9240–1.
- Bergren MR, Makarov NS, Ramasamy K, Jackson A, Guglielmetti R, Mcdaniel HJAEL. High-performance CuInS₂ quantum dot laminated glass luminescent solar concentrators for windows. *ACS Energy Lett.* 2018;3(3):520–5.
- De Trizio L, Prato M, Genovese A, Casu A, Povia M, Simonutti R, et al. Strongly fluorescent quaternary Cu–In–Zn–S nanocrystals prepared from Cu_{1-x}InS₂ nanocrystals by partial cation exchange. *Chem Mater.* 2012;24(12):2400–6.
- Stroyuk O, Weigert F, Raevskaya A, Spranger F, Würth C, Resch-Genger U, et al. Inherently broadband photoluminescence in Ag–In–S/ZnS quantum dots observed in ensemble and single-particle studies. *J Phys Chem C.* 2019;123(4):2632–41.
- Hines MA, Guyot-Sionnest PJC. Synthesis and characterization of strongly luminescing ZnS-capped CdSe nanocrystals. *J Phys Chem C.* 2010;27(19):468–71.
- Sakai R, Onishi H, Ido S, Furumi SJN. Effective Mn-doping in AgInS₂/ZnS core/shell nanocrystals for dual photoluminescent peaks. *Nanomaterials.* 2019;9(2):263.
- Mao B, Chuang C-H, Wang J, Burda C. Synthesis and photophysical properties of ternary I–III–VI AgInS₂ nanocrystals: intrinsic versus surface states. *J Phys Chem C.* 2011;115(18):8945–54.
- Cai C, Zhai L, Ma Y, Zou C, Zhang L, Yang Y, et al. Synthesis of AgInS₂ quantum dots with tunable photoluminescence for sensitized solar cells. *J Power Sources.* 2017;341:11–8.

18. Talapin DV, Lee J-S, Kovalenko MV, Shevchenko EV. Prospects of colloidal nanocrystals for electronic and optoelectronic applications. *Chem Rev.* 2010;110(1):389–458.
19. Zhang K, Lv S, Lu M, Tang D. Photoelectrochemical biosensing of disease marker on p-type Cu-doped Zn_{0.3}Cd_{0.7}S based on RCA and exonuclease III amplification. *Biosens Bioelectron.* 2018;117:590–6.
20. Zhang K, Lv S, Zhou Q, Tang D. CoOOH nanosheets-coated g-C₃N₄/CuInS₂ nanohybrids for photoelectrochemical biosensor of carcinoembryonic antigen coupling hybridization chain reaction with etching reaction. *Sensors Actuators B Chem.* 2020;307:127631.
21. Montalti M, Cantelli A, Battistelli G. Nanodiamonds and silicon quantum dots: ultrastable and biocompatible luminescent nanoprobes for long-term bioimaging. *Chem Soc Rev.* 2015;44(14):4853–921.
22. Tsuji I, Kato H, Kobayashi H, Kudo A. Photocatalytic H₂ evolution reaction from aqueous solutions over band structure-controlled (AgIn)_xZn₂(1-x)S₂ solid solution photocatalysts with visible-light response and their surface nanostructures. *J Am Chem Soc.* 2004;126(41):13406–13.
23. Stroyuk O, Raevskaya A, Spranger F, Selyshchev O, Dzhanan V, Schulze S, et al. Origin and dynamics of highly efficient broadband photoluminescence of aqueous glutathione-capped size-selected Ag–In–S quantum dots. *J Phys Chem C.* 2018;122(25):13648–58.
24. Long X, Zhang F, He Y, Hou S, Zhang B, Zou G. Promising anodic electrochemiluminescence of nontoxic core/shell CuInS₂/ZnS nanocrystals in aqueous medium and its biosensing potential. *Anal Chem.* 2018;90(5):3563–9.
25. Zhang B, Zhang F, Zhang P, Shen D, Gao X, Zou G. Ultrasensitive electrochemiluminescent sensor for microRNA with multinary Zn–Ag–In–S/ZnS nanocrystals as tags. *Anal Chem.* 2019;91(5):3754–8.
26. Zhang X, Tan X, Zhang B, Miao W, Zou G. Spectrum-based electrochemiluminescent immunoassay with ternary CdZnSe nanocrystals as labels. *Anal Chem.* 2016;88(13):6947–53.
27. Xiong W-W, Yang G-H, Wu X-C, Zhu J-J. Aqueous synthesis of color-tunable CuInS₂/ZnS nanocrystals for the detection of human interleukin 6. *ACS Appl Mater Interfaces.* 2013;5(16):8210–6.
28. Martynenko IV, Kusic D, Weigert F, Stafford S, Donnelly FC, Evstigneev R, et al. Magneto-fluorescent microbeads for bacteria detection constructed from superparamagnetic Fe₃O₄ nanoparticles and AIS/ZnS quantum dots. *Anal Chem.* 2019;91(20):12661–9.
29. Wujian M. Electrogenerated chemiluminescence and its biorelated applications. *Chem Rev.* 2008;108(7):2506–53.
30. Hesari M, Ding Z. A grand avenue to au nanocluster electrochemiluminescence. *Acc Chem Res.* 2017;50(2):218–30.
31. He Y, Zhang F, Zhang B, Zou G. Dichroic mirror-assisted electrochemiluminescent assay for simultaneously detecting wild-type and mutant p53 with photomultiplier tubes. *Anal Chem.* 2018;90(8):5474–80.
32. Liang X, Han H, Ma Z. pH responsive amperometric immunoassay for carcinoma antigen 125 based on hollow polydopamine encapsulating methylene blue. *Sensors Actuators B Chem.* 2019;290:625–30.
33. Wang S, Ge L, Yan M, Yu J, Song X, Ge S, et al. 3D microfluidic origami electrochemiluminescence immunodevice for sensitive point-of-care testing of carcinoma antigen 125. *Sensors Actuators B Chem.* 2013;176:1–8.
34. Samadi Pakchin P, Ghanbari H, Saber R, Omidi Y. Electrochemical immunosensor based on chitosan-gold nanoparticle/carbon nanotube as a platform and lactate oxidase as a label for detection of CA125 on comarker. *Biosens Bioelectron.* 2018;122:68–74.
35. Büyüktiryaki S, Say R, Denizli A, Ersöz A. Phosphoserine imprinted nanosensor for detection of cancer antigen 125. *Talanta.* 2017;167:172–80.
36. Torati SR, Kasturi KCSB, Lim B, Kim C. Hierarchical gold nanostructures modified electrode for electrochemical detection of cancer antigen CA125. *Sensors Actuators B Chem.* 2017;243:64–71.
37. Wang M, Hu M, Li Z, He L, Song Y, Jia Q, et al. Construction of Tb-MOF-on-Fe-MOF conjugate as a novel platform for ultrasensitive detection of carbohydrate antigen 125 and living cancer cells. *Biosens Bioelectron.* 2019;142:111536.

Publisher's note Springer Nature remains neutral with regard to jurisdictional claims in published maps and institutional affiliations.